Chain cleavage of bioinspired bacterial membranes photoinduced by eosin decyl ester

Lucas G. Moreira[1], Alexandre M. Almeida Jr.[1], Sabrina A. Camacho[1,2], Bianca M. Estevão[2,3], Osvaldo N. Oliveira Jr.[2], Pedro H. B. Aoki[1]

[1] School of Sciences, Humanities and Languages, São Paulo State University (UNESP), Assis, SP, 19806-900, Brazil

[2] IFSC, São Carlos Institute of Physics, University of São Paulo (USP), São Carlos, SP 13566-590, Brazil

[3] Department of Chemistry, State University of Maringá (UEM), Maringá, PR, 87020-900, Brazil

Abstract

Photodynamic therapy (PDT) is promising for bacterial inactivation since cellular internalization of photosensitizers (PS) is not crucial for the treatment effectiveness. Photoinduced damage in the lipid envelope may already induce microbial inactivation, which requires PS capable of easily penetrating into the membrane. Herein, we report on the insertion of the PS eosin decyl ester (EosDec) into Langmuir films of 1,2-dioleoyl-sn-glycero-3-phosphoethanolamine (DOPE), 1,2-dioleoyl-sn-glycero-3-phospho-(1′-rac-glycerol) (DOPG) and cardiolipin (CLP) used as mimetic systems of bacterial membranes. Surface pressure isotherms and polarization-modulated infrared reflection absorption spectroscopy (PM-IRRAS) indicated that the hydrophobic nature of EosDec favored deeper penetration in all the phospholipid monolayers. The incorporation of EosDec led to monolayer expansion, especially in the anionic DOPG and CLP owing to repulsive electrostatic interactions, and induced disorder in the lipid chains. Light irradiation of DOPE, DOPG and CLP monolayers containing EosDec increased the rate of material loss to the subphase, which is attributed to cleavage of lipid chains triggered by contact-dependent reactions between excited states of EosDec and lipid unsaturations. The latter is key for membrane permeabilization and efficiency in microbial inactivation.

Keywords: Langmuir monolayers, cell membranes, photosensitizers, photodynamic therapy, bacterial inactivation

Introduction

Infectious diseases caused by drug-resistant microorganisms are major concerns to public health and global economics[1]. Bacterial resistance may originate from pre-existing innate mechanisms and acquired genetic materials, and intensified by the indiscriminate use[2] and improper disposal of antibiotics[3]. Gram-negative bacteria, in particular, have an outer membrane with lipopolysaccharides (LPS), which makes them less susceptible to the action of antibiotics[4–6] and demand alternative therapeutics[7–9]. An alternative is photodynamic therapy (PDT) for which cell internalization is not mandatory for bacterial inactivation[10–13]. PDT is based on a local or systemic administration of a photosensitizer (PS), further irradiated with appropriate wavelength to produce reactive oxygen species (ROS), which are cytotoxic to biological tissues, DNA, organelles, proteins, and lipid membranes[14–16]. Basically, the PS absorbs energy to reach its excited singlet state (^{1}PS*) and undergoes intersystem crossing to the triplet state (^{3}PS*), from which ROS can be formed via type I or type II reactions[17–19]. Created from the energy transfer to the molecular oxygen ($^3O_2$), singlet oxygen ($^1O_2$) is the main result of type II reaction, relevant for PDT. The short lifetime restricts $^1O_2$ diffusion and confines the oxidation reactions to the PS vicinity. Therefore, PS location in the biological target is key to the photooxidation reactions and to the PDT success.

Cell membranes are the main targets of $^1O_2$ attack, which may lead to lipid hydroperoxidation as a result of ene reactions with alkenes containing allylic hydrogens[20–22]. Since phosphatidylcholines (PC) are major components of healthy eukaryotic cell membranes,[23–27] we have used them in Langmuir monolayers as simplified models, and showed that hydrophilic hydroperoxides created in the hydrophobic core of phospholipids disrupt the hydrophilic-hydrophobic balance of the monolayer leading to an overall surface area increase[21,22]. We have hypothesized that the PS binding site can modulate the photochemical outcome from hydroperoxidation to the chain cleavage and

membrane permeabilization, triggered by contact-dependent reactions with excited states of PSs that penetrate deeper into the monolayer[28,29]. However, the limited penetration of water-soluble PS into the monolayers do not afford control over such modulation, which has prompted a search for PSs whose increased hydrophobicity allows effective insertion towards the lipid chains[17,30].

This challenge has been addressed with the synthesis of xanthene ester derivatives containing alkyl groups, which keep their light absorption, low toxicity and high quantum yield (Φ_Δ) for $^1O_2$[17,31]. The quantum yield is maintained owing to the halogen substitutes[31] that increase the yield of intersystem crossing to $^3PS^*$ [32,33]. For instance, eosin decyl ester (EosDec) has high $\Phi_\Delta{}^1O_2$ (0.38), excitation under visible light (λ=526 nm) and partition coefficient (1.84) of hydrophobic compounds[17]. Herein, we probe the molecular-level effects of the EosDec insertion into simplified model systems of bacterial membranes made with Langmuir monolayers of 1,2-dioleoyl-snglycero-3-phosphoethanolamine (DOPE), 1,2-dioleoyl-snglycero-3-phospho-1'-rac-glycerol (DOPG) and cardiolipin (CLP). Photooxidation effects were investigated using surface pressure (π) *vs* mean molecular area (A) isotherms and polarization-modulated infrared reflection absorption spectroscopy (PM-IRRAS). As we shall demonstrate, the hydrophobic character of EosDec is key for deeper penetration into the monolayers and contact-dependent processes that yield chain cleavage and possible membrane permeabilization.

Experimental Section

Materials

The phospholipids 1,2-dioleoyl-*sn*-glycero-3-phosphoethanolamine (DOPE), 1,2-dioleoyl-*sn*-glycero-3-phospho-(1'-rac-glycerol) (DOPG) and cardiolipin (CLP, > 99%) were acquired from Avanti Polar Lipids. The photosensitizer eosin decyl ester (EosDec) was synthesized following previous-established protocols[17]. The molecular structures of DOPE, DOPG, CLP and the xanthene derivative EosDec are displayed in Figure 1a. The materials were used as received, with no further purification. Ultrapure water (resistivity = 18.2 MΩ·cm) from a Milli-Q equipment (model Direct-Q® 3UV) was employed as subphase in the Langmuir trough. Chloroform ($CHCl_3$, 99,0 ~ 99,4%) from Sigma-Aldrich was used to dissolve the lipids and EosDec.

Langmuir films fabrication

Langmuir monolayers of phospholipids may be used as simplified models of only half of a cell membrane. They are nevertheless useful since the lateral packing and membrane composition can be controlled, and molecular-level interaction can be inferred with *in situ* measurements, including with PM-IRRAS which permitted determination of the action mechanism of biologically-relevant molecules[22,28,34–39]. The Langmuir films were fabricated in a Langmuir trough (KSV-NIMA / KN 2002) by spreading each phospholipid solution (10^{-3} mol/L) on an aqueous subphase at room temperature (23ºC). The same methodology was applied for neat EosDec, whereas for the EosDec:lipid films we first spread the phospholipid solution and then the EosDec solution immediately afterward. The solvent was allowed to evaporate for 15 min prior to the barriers compression at a constant rate of 5 mm/min. The surface pressure (π) *versus* mean molecular area ($Å^2$) isotherms were recorded with the pressure measured using the Wilhelmy method with a platinum plate. No other procedure was adopted to avoid uncontrolled oxidation from the

environment[33], but the reproducibility of the isotherms was ascertained by repeating the experiments and finding that the surface pressure varied within only ± 2 mN/m for a given area.

Irradiation experiments

The co-spread monolayers EosDec:DOPE (1:5), EosDec:DOPG (1:5) and EosDec:CLP (1:2) were irradiated at 30 mN/m with a LED source (ca. 530 nm, BRIWAX FFG/50 W) positioned 15 cm above the monolayer interface, as sketched in Figure 1b. Polarization-modulated infrared reflection-absorption spectroscopy (PM-IRRAS) was carried out in a KSV PMI550 (KSV, Finland) on neat monolayers of DOPE, DOPG, CLP and EosDec at 30 mN/m. The co-spread EosDec:DOPE (1:5), EosDec:DOPG (1:5) and EosDec:CLP (1:2) monolayers were also characterized, before and after irradiation. The experiments were performed from 1000 to 3100 cm^{-1} (incidence angle = 81° and resolution = 8 cm^{-1}). The spectral reproducibility was checked by measuring the monolayers at least three times to ensure that the changes observed are not associated with spectral variability.

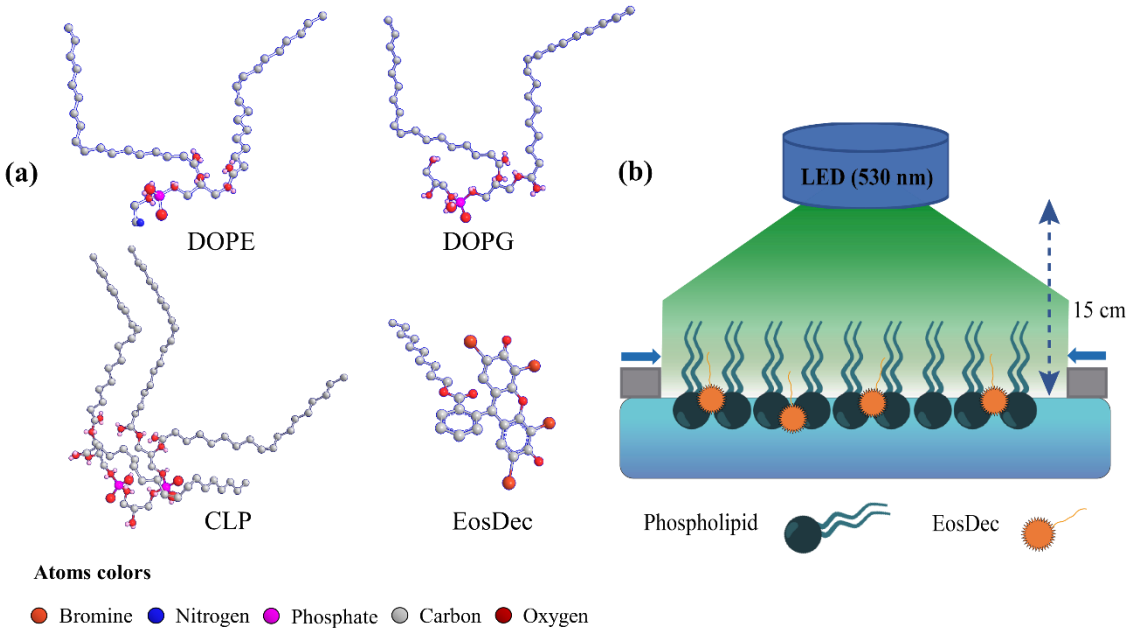

Figure 1. (a) Molecular structures of DOPE, DOPG, CLP, and the xanthene derivative EosDec. (b) Illustration of the irradiation experiment. The LED is placed 15 cm above the co-spread film, allowing for irradiation of the entire surface.

Results and discussion

EosDec incorporation into DOPE and DOPG monolayers

The π-A isotherms for neat DOPE, DOPG, EosDec and the co-spread monolayers at 1:5 and 1:1 (EosDec:lipid) molecular ratios are displayed in Figure 2. The partition coefficient of 1.84 provides a hydrophobic character to EosDec[17], which allows for Langmuir film formation with a high slope in the π-A isotherm and collapse pressure around 45 mN/m. The extrapolated area to zero pressure to the slope at 30 mN/m of 73 $Å^2$ is small and suggests a highly packed monolayer owing to the π-π interactions between the xanthene rings[40], which is similar to what was observed for the porphyrin derivatives ZnPP[41], ZnPPIX-DME[42] and Hemin[43]. The increase of EosDec molecular ratio up to 1:1 (EosDec:lipid) displaces the π-A isotherms to larger molecular areas due to the increasing amount of EosDec molecules incorporated by the phospholipid monolayers. Table 1 shows the change in relative molecular area $[(A - A_o)/A_o]$ as a function of EosDec molecular ratio. The change is larger for EosDec:DOPG than for EosDec:DOPE monolayers, independent of the EosDec amount. Both phospholipids have the same aliphatic chain, and therefore the polar head groups affect EosDec incorporation, probably because of repulsion with DOPG anionic polar groups which would not exist for the zwitterionic DOPE[44–47]. In the condensed phase, the slope of the isotherm for EosDec:DOPG (1:1) decreased, with a slight increase in the collapse pressure, which did not occur for EosDec:DOPE monolayers. The results for dianionic cardiolipin (CLP) monolayers are similar to those of DOPG, whose data and discussion are given as supplementary material (Figures S1 and S3). In addition, the mean molecular area *vs* the molar fraction of EosDec (X_{EosDec})[48,49] was analyzed for DOPE, DOPG and CLP co-spread monolayers (Figure S2 in the Supporting Information), confirming the monolayers expansion.

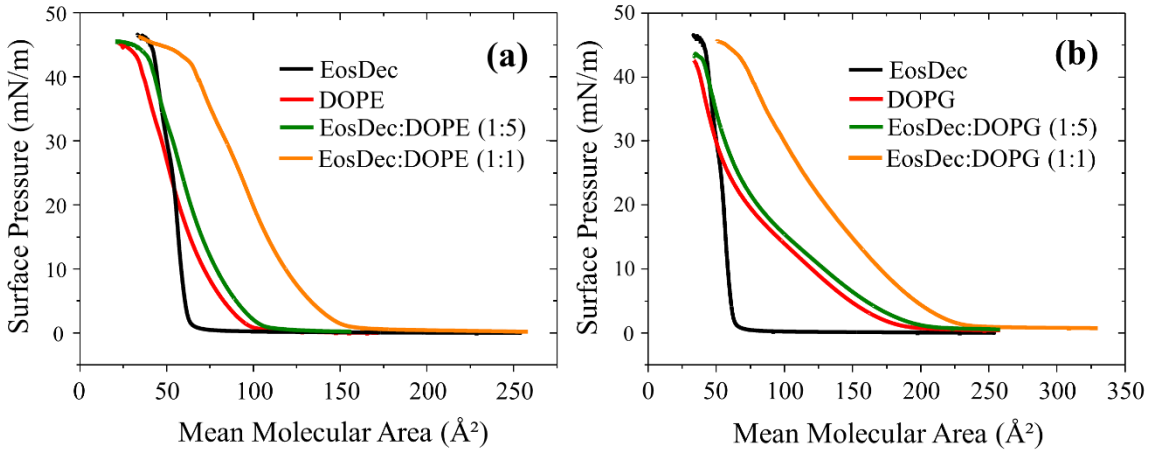

Figure 2. π-A isotherms of (a) DOPE, (b) DOPG and co-spread monolayers at 1:1 and 1:5 (EosDec:lipid) molecular ratio. The π-A isotherm of neat EosDec (black curve) is provided as control.

Table 1. Relative shifts in area per phospholipid $[(\frac{A - A_o}{A_o})\ x\ 100)]$, where A_o and A are the extrapolated areas at 30 mN/m for the π-A isotherms of neat and co-spread monolayers, respectively.

EosDec:phospholipid ratio	**Relative shift in the isotherm**	
	DOPE	DOPG
1:1	70.2 % ± 0.9 %	85.7 % ± 2.8 %
1:5	8.5 % ± 2.1 %	11.0 % ± 1.5 %

The molecular-level effects induced by EosDec incorporation into the lipid films were assessed here using polarization-modulated infrared reflection-absorption spectroscopy (PM-IRRAS). Table 2 brings the assignments of PM-IRRAS bands and displacements caused by EosDec incorporation and further irradiation. The spectra acquired for neat DOPE, EosDec and the co-spread EosDec:DOPE (1:5) monolayers are shown in Figure 3. (The PM-IRRAS data for CPL are discussed in the Supporting Information.) EosDec causes a minor effect over the DOPE head groups (Figure 3a) by increasing the band intensity at 1026 cm^{-1} and 1165 cm^{-1}, assigned to $\upsilon(C–O–PO_2^-)$ and $\upsilon_{as}(C–O–C)$, respectively. The vibrational modes of the xanthene ring[17,42] appear at 1520 cm^{-1} and 1450 cm^{-1}, confirming the presence of EosDec in the monolayer. In phosphatidylethanolamine

membranes, hydrogen bonds between the phosphate and amine groups of adjacent molecules generate an inter-phospholipid network that decreases the availability of phosphates to establish new interactions[50]. Therefore, electrostatic interactions with the anionic EosDec are impaired, which is consistent with the slight modifications observed in the phosphate vibrational modes. As for the bands associated with the chains in Figure 3b, $\upsilon_s(CH_2)$ at 2854 cm^{-1} is shifted to 2840 cm^{-1} with increased intensity while $\upsilon_{as}(CH_3)$ at 2952 cm^{-1} had its intensity reduced upon EosDec incorporation. The ratio between the band intensity of the symmetric and antisymmetric CH_2 stretching ($I_{\upsilon_s(CH_2)}/I_{\upsilon_{as}(CH_2)}$) increased from 0.50 to 1.08 indicating a decreased order of the chains[51]. This high impact on the tails may suggest penetration of EosDec molecules into the alkyl chains, as depicted in Figure 3c. Similar findings were observed for antimicrobial agents with amphiphilic character incorporated into saturated PE monolayers[52,53].

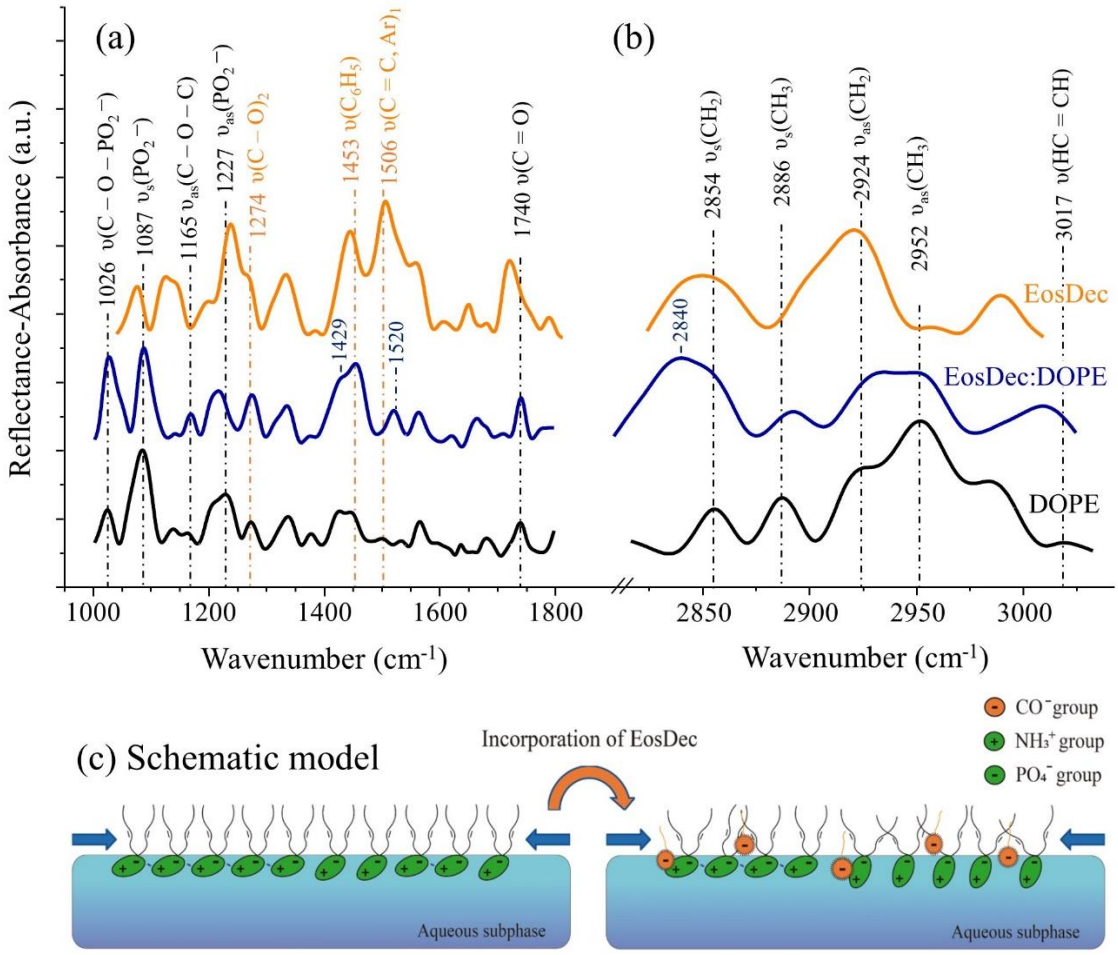

Figure 3. PM-IRRAS spectra of the (a) polar heads and (b) alkyl tails acquired for neat DOPE, EosDec and co-spread EosDec:DOPE (1:5) films at 30 mN/m on aqueous subphase. (c) Proposed model for the interaction between EosDec – DOPE. The model is merely illustrative of the molecular-level interactions inferred from the monolayer characterization.

The bands assigned to the phosphate groups are more disturbed in DOPG monolayers owing to the stronger electrostatic repulsion with the anionic EosDec. Figure 4a shows that the incorporation of EosDec shifts $\upsilon(C–O–PO_2^-)$ from 1057 cm^{-1} to 1023 cm^{-1}, $\upsilon_{as}(PO_2^-)$ from 1226 to 1246 cm^{-1} and increases $\upsilon_s(PO_2^-)$ intensity at 1100 cm^{-1}. It is likely that the interaction with EosDec has affected the hydrogen bonds with the surrounding water[54,55], leading to dehydration of phosphate groups[56]. The C=C stretching mode at 1544 cm^{-1} is due to the xanthene ring and confirms EosDec incorporation into the DOPG monolayer. The C=C and C_6H_5 stretching modes at 1506 cm^{-1} and 1445 cm^{-1} in the neat EosDec spectrum shifted to 1483 cm^{-1} and 1433 cm^{-1} in the co-spread EosDec:DOPG

(1:5) film. The band position of the alky chains in Figure 4b remains unaltered except for the $I_{\upsilon_s(CH_2)}/I_{\upsilon_{as}(CH_2)}$ ratio which increased from 0.30 to 1.23 owing to the disordering of the chains[51]. Considering these modifications with the larger areas in π-A isotherms (Table 1), one may conclude that DOPG monolayers are significantly more affected by EosDec incorporation. Electrostatic repulsion between the DOPG anionic portions have been increased by the insertion of anionic EosDec molecules, thus favoring the monolayer expansion and chain disordering, as indicated in Figure 4c.

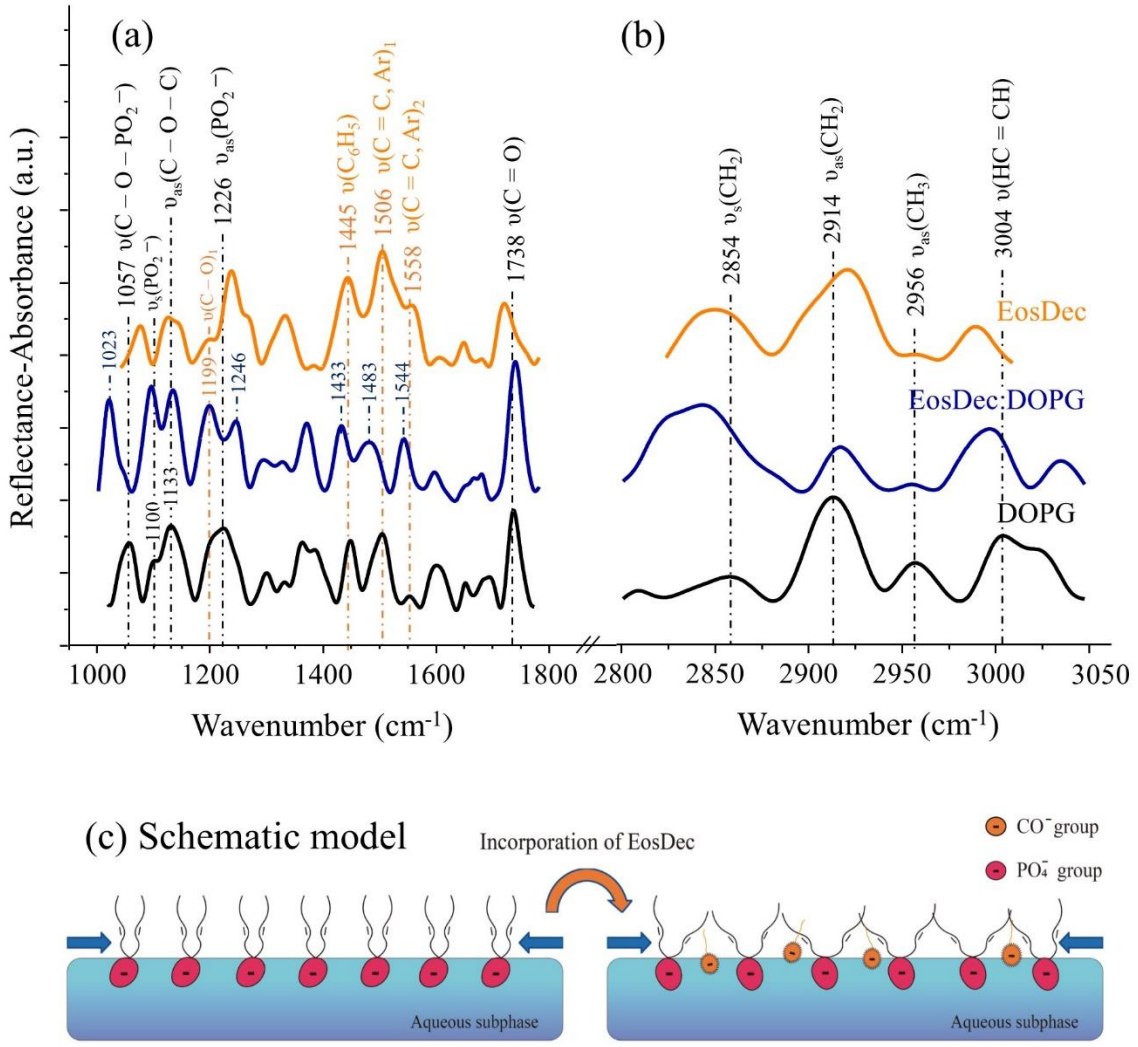

Figure 4. PM-IRRAS spectra of the (a) polar heads and (b) alkyl tails acquired for neat DOPG, EosDec and co-spread EosDec:DOPG (1:5) films at 30 mN/m on aqueous subphase. (c) Proposed model for the interaction between EosDec – DOPG. As in Figure 3(c), this schematic drawing is a mere illustration of the interactions.

Table 2. Assignments of the main bands of neat DOPE, DOPG, EosDec and the co-spread EosDec:DOPE (1:5), EosDec:DOPG (1:5) Langmuir monolayers.

Assignments	DOPE (cm^{-1})			DOPG (cm^{-1})			EosDec (cm^{-1})
	Water	1:5	Irrad	Water	1:5	Irrad	Water
υ(HC=CH)	3017	3009	3009	3004	2997	3008	-
$\upsilon_{as}(CH_3)$	2952	2952	2952	2956	2956	2975	2958
$\upsilon_{as}(CH_2)$	2924	2932	2924	2914	2917	2917	2921
$\upsilon_{s}(CH_3)$	2886	2892	2892	-	-	-	-
$\upsilon_{s}(CH_2)$	2854	2840	2862	2854	2846	2846	2850
υ(C=O)	1740	1740	1740	1738	1738	1745	1720
υ(C=C, Aromatic)$_2$	-	1565	1565	-	1544	1542/ 1565	1558
υ(C=C, Aromatic)$_1$	-	1520	1506	-	1483	1470	1506
$\upsilon(C_6H_5)$	-	1453	1453	-	1433	1434	1445
υ(C–O)$_2$	-	1274	1274	-	-	-	1267
$\upsilon_{as}(PO_2^-)$	1227	1219	1219	1226	1246	1246	-
υ(C–O)$_1$	-	-	-	-	1199	1206	1198
υ_{as}(C–O–C)	1165	1169	1169	1133	1133	1133	-
$\upsilon_{s}(PO_2^-)$	1087	1087	1087	1100	1096	1096	-
υ(C–O–PO_2^-)	1026	1026	1026	1057	1023	1023	-

*1:5 and 1:2 = EosDec:lipid; Irrad = Irradiated film

EosDec photoactivation

Photochemical reactions were monitored by measuring the surface area evolution of irradiated EosDec:DOPE (1:5), EosDec:DOPG (1:5) co-spread monolayers kept at 30 mN/m, as shown in Figure 5a and 5b. From subsidiary experiments we observed that irradiation has no effect on neat DOPE, DOPG and CLP monolayers, whose profiles do not statistically differ from the nonirradiated EosDec containing monolayers. A decrease in surface area is observed for all nonirradiated monolayers and is associated with the loss of material to the subphase generated by uncontrolled oxidation via reactive oxygen species (ROS) from the environment[33,57]. The anionic nature of DOPG increases

monolayer instability and the material loss rate, which is consistent with previous findings[58]. The slope of the irradiated monolayers is higher than for nonirradiated monolayers suggesting an enhanced material loss to the subphase, which was also noted for ozone oxidation[59,60] and UV damage[58]. The higher stability of nonirradiated DOPE monolayer is the origin of the largest relative decrease in area, which at the end of 100 min of irradiation is reduced by 28 % ± 6% against 19% ± 5% for DOPG monolayers. As expected, the results for the negatively charged CLP in Figure S4 are similar to those of DOPG.

The energy transfer from excited states of EosDec to the molecular oxygens (O_2) generates singlet oxygen ($^1O_2$) species that can further react with lipid unsaturations. We have already shown that the tailless eosin Y adsorbs on phosphatidylcholine moieties by electrostatic interactions, with limited penetration into the chain region[22]. Upon irradiation, the $^1O_2$ created in the vicinity of the hydrophilic groups were able to react with the chain unsaturation and form hydroperoxides. Their hydrophilic character led these groups toward the water interface, resulting in the overall surface area increase of the monolayer. There is also evidence that molecular-level interactions of photosensitizers with lipid monolayers modulate the photochemical reactions[20–22,28]. For instance, deeper penetration of the cationic toluidine blue-O (TBO) into the chain region of phosphatidylglycerol monolayers was observed owing to stronger attractive electrostatic interactions. The proximity with the chains allowed the permeabilization of the membranes by contact-dependent reactions between excited states of TBO and unsaturations or previously formed hydroperoxides[28].

The hydrophobic character of EosDec allows insertion into the aliphatic chains of the phospholipids, as inferred from the PM-IRRAS data. Therefore, not only would $^1O_2$ be produced nearby the unsaturated region, and consequently favor phospholipid hydroperoxidation, but also the proximity of PS molecules would enable the generation

of aldehydes by contact-dependent processes, as shown in Figure 6. The latter induce cleavage of lipid tails, which may be the source of material loss in all monolayers. Indeed, the modifications in the PM-IRRAS spectra of irradiated monolayers in Figure 5 are consistent with such oxidative reactions. For instance, the panel on the right of Figure 5a shows that the $\upsilon(C–O–PO_2^-)$ band intensity at 1026 cm^{-1} is reduced on the irradiated EosDec:DOPE (1:5). Moreover, the bands due to carbonyl ester groups at 1169 cm^{-1} and 1740 cm^{-1} had their intensity increased, indicating modifications in the hydration of the lipid polar region[61]. The vibrational modes of the xanthene rings were also affected with a decreased intensity of the phenyl group at 1429 and 1453 cm^{-1}. In addition, the υ(C=C, Aromatic)$_1$ band at 1520 cm^{-1} shifted to 1506 cm^{-1} and the intensity of υ(C=C, Aromatic)$_2$ at 1565 cm^{-1} increased[17,42]. As for the tails, the $\upsilon_s(CH_2)$ band at 2840 cm^{-1} shifted to 2862 cm^{-1} with decreased intensity while $\upsilon_{as}(CH_3)$ at 2952 cm^{-1} had the intensity significantly increased. The $I_{\upsilon_s(CH_2)}/I_{\upsilon_{as}(CH_2)}$ ratio was barely modified suggesting that the chain disorder induced by EosDec insertion was maintained upon irradiation.

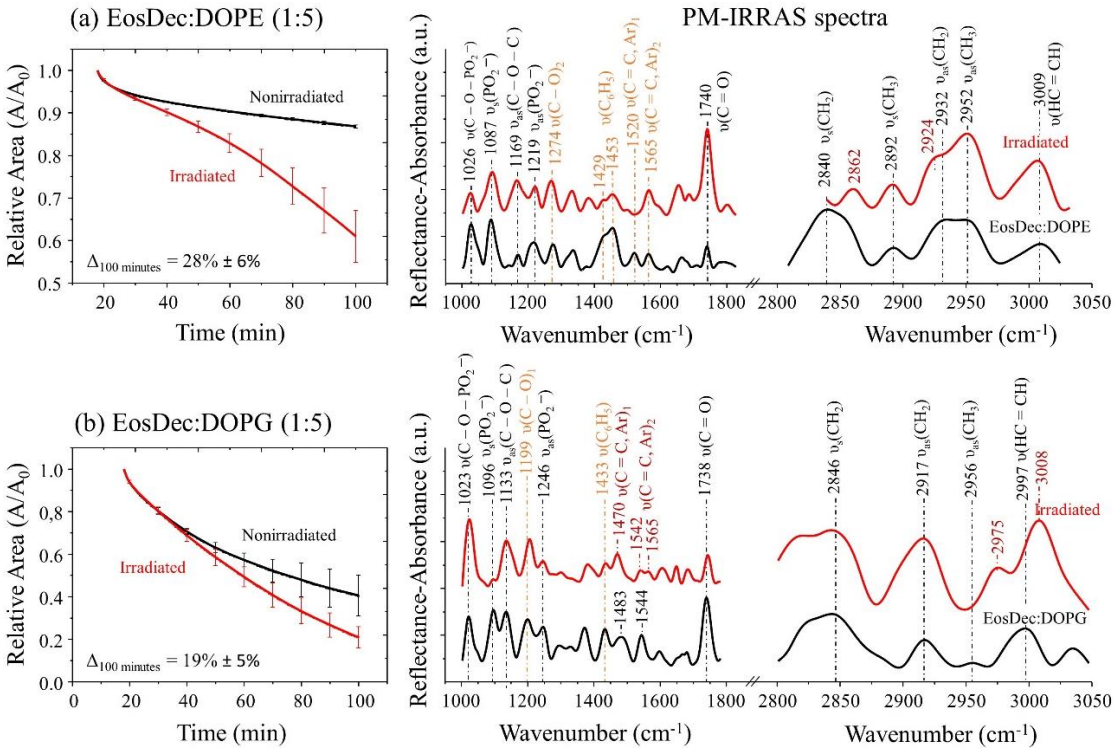

Figure 5. Relative area (A/A_0) progress of the nonirradiated (black curves) and irradiated (red curves) (a) EosDec:DOPE (1:5) and (b) EosDec:DOPG (1:5) monolayers. A_0 is the

extrapolated area of the phospholipid isotherms at 30 mN/m down to zero pressure. The PM-IRRAs spectra recorded for nonirradiated and irradiated co-spread monolayers are provided in the panel on the right.

Stronger modifications were observed in the phosphate region of irradiated EosDec:DOPG (1:5) monolayers, shown in Figure 5b. The intensity of $\upsilon(C–O–PO_2^-)$ band at 1023 cm^{-1} decreased while an increase was observed for $\upsilon_s(PO_2^-)$ and $\upsilon_{as}(PO_2^-)$ at 1096 and 1246 cm^{-1}. In addition, the intensity of the carbonyl ester group band at 1738 cm^{-1} decreased. The xanthene vibrational modes were affected in a similar way to that for irradiated EosDec:DOPE (1:5) monolayer. The $\upsilon(C=C, \text{aromatic})_1$ band shifted from 1483 to 1470 cm^{-1}, the $\upsilon(C=C, \text{aromatic})_2$ band at 1544 cm^{-1} split into two bands at 1542 and 1565 cm^{-1}, and the C_6H_5 stretching band at 1433 cm^{-1} had its intensity reduced[17,42]. Such modifications are consistent with the report on lipid hydroperoxidation[22], which can impact the organization of EosDec within the monolayer. The chains were also affected with an increase in the $\upsilon_{as}(CH_2)$ band at 2917 cm^{-1}, resulting in a slight decrease in the chains disorder with a reduced $I_{\upsilon_s(CH_2)}/I_{\upsilon_{as}(CH_2)}$ ratio[51]. Besides, the $\upsilon_{as}(CH_3)$ band shifted from 2956 to 2975 cm^{-1} and the υ(HC=CH) band shifted from 2997 to 3008 cm^{-1}. The presence of υ(HC=CH) band in both EosDec:DOPE and EosDec:DOPG irradiated monolayers suggests the solubilization of the cleaved lipids in the subphase, leaving the uncleaved lipids at the interface to be probed.

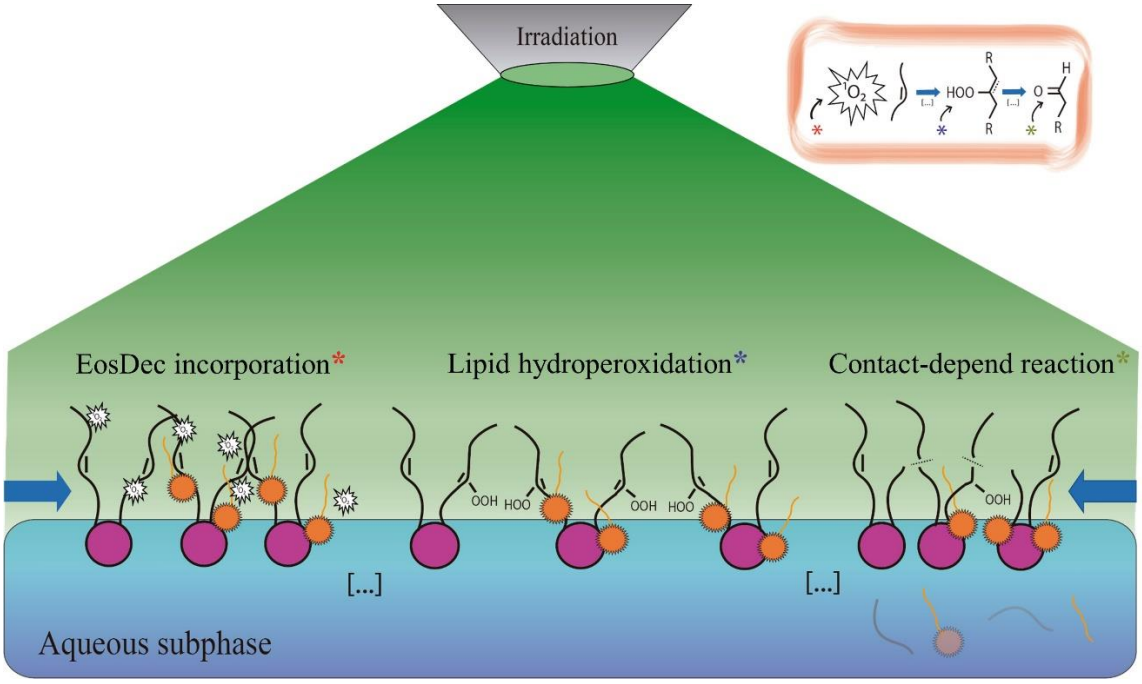

Figure 6. Scheme of the alkyl chains cleavage under contact reactions between excited states of EosDec and unsaturations.

Conclusions

Langmuir films of DOPE, DOPG and CLP phospholipids were used here as simplified models of bacterial cell membranes to unravel the molecular-level interactions with the photosensitizer eosin decyl ester (EosDec) and further photoinduced effects. EosDec incorporation affected the polar heads region, especially for the anionic DOPG and CLP owing to electrostatic repulsion that led to larger monolayer expansion. Furthermore, the hydrophobic nature of EosDec allowed deeper penetration into the monolayers causing an increase in chain disorder. The photoactivation of the incorporated EosDec decreased the stability of DOPE, DOPG and CLP monolayers, and induced an increased loss of material to the subphase, bringing chemical and physical disturbances to the monolayer. The penetration of EosDec into the hydrophobic core of the monolayer favored contact-dependent reactions between the excited triplet state of EosDec and lipid unsaturations or hydroperoxides previously formed, resulting in the cleavage of the chains. These findings contribute to the understanding on how the molecular-level interactions with photosensitizers impact the photosensitization outcome in model systems of bacterial membranes, which are relevant for photodynamic therapy in microbial inactivation.

Acknowledgments

This work was supported by São Paulo Research Foundation (FAPESP 2013/14262-7, 2018/16713-0, 2018/14692-5 and 2018/22214-6), INEO and National Council for Scientific and Technological Development (CNPq Universal 403713/2016-1). We thank Diogo S. Pellosi and Dr. Wilker Caetano for their assistance with EosDec. Lucas Gontijo Moreira is thankful for his scholarship provided by FAPESP (2018/13021-0).

Conflicts of interest

There are no conflicts to declare.

References

(1) Basak, S.; Singh, P.; Rajurkar, M. Multidrug Resistant and Extensively Drug Resistant Bacteria: A Study. *J. Pathog.* **2016**, *2016*, 1–5. https://doi.org/10.1155/2016/4065603.

(2) Mishra, R. P. N.; Oviedo-Orta, E.; Prachi, P.; Rappuoli, R.; Bagnoli, F. Vaccines and Antibiotic Resistance. *Curr. Opin. Microbiol.* **2012**, *15* (5), 596–602. https://doi.org/https://doi.org/10.1016/j.mib.2012.08.002.

(3) Grenni, P.; Ancona, V.; Barra Caracciolo, A. Ecological Effects of Antibiotics on Natural Ecosystems: A Review. *Microchem. J.* **2017**. https://doi.org/10.1016/j.microc.2017.02.006.

(4) Neu, H. C. The Crisis in Antibiotic Resistance. *Science (80-.).* **1992**, *257* (5073), 1064 LP-1073. https://doi.org/10.1126/science.257.5073.1064.

(5) Delcour, A. H. Outer Membrane Permeability and Antibiotic Resistance. *Biochim. Biophys. Acta - Proteins Proteomics* **2009**, *1794* (5), 808–816. https://doi.org/https://doi.org/10.1016/j.bbapap.2008.11.005.

(6) Zgurskaya, H. I.; Rybenkov, V. V; Krishnamoorthy, G.; Leus, I. V. Trans-Envelope Multidrug Efflux Pumps of Gram-Negative Bacteria and Their Synergism with the Outer Membrane Barrier. *Res. Microbiol.* **2018**, *169* (7), 351–356. https://doi.org/https://doi.org/10.1016/j.resmic.2018.02.002.

(7) Huang, Y.; Tanaka, M.; Vecchio, D.; Garcia-diaz, M.; Chang, J.; Morimoto, Y.; Hamblin, M. R. Photodynamic Therapy Induces an Immune Response against a Bacterial Pathogen. *Expert Rev Clin Immunol* **2012**, *8* (5), 479–494. https://doi.org/10.1586/eci.12.37.Photodynamic.

(8) Simões, M.; Bennett, R. N.; Rosa, E. A. S. Understanding Antimicrobial Activities of Phytochemicals against Multidrug Resistant Bacteria and Biofilms. *Nat. Prod. Rep.* **2009**, *26* (6), 746–757. https://doi.org/10.1039/B821648G.

(9) Chan, B. K.; Abedon, S. T.; Loc-Carrillo, C. Phage Cocktails and the Future of Phage Therapy. *Future Microbiol.* **2013**, *8* (6), 769–783. https://doi.org/10.2217/fmb.13.47.

(10) Hamblin, M. R.; Hasan, T. Photodynamic Therapy: A New Antimicrobial Approach to Infectious Disease? *Photochem. Photobiol. Sci.* **2004**, *3* (5), 436–450. https://doi.org/10.1039/B311900A.

(11) Demidova, T. N.; Hamblin, M. R. Photodynamic Therapy Targeted to Pathogens. *Int. J. Immunopathol. Pharmacol.* **2004**, *17* (3), 245–254. https://doi.org/10.1177/039463200401700304.

(12) Topaloglu, N.; Gulsoy, M.; Yuksel, S. Antimicrobial Photodynamic Therapy of Resistant Bacterial Strains by Indocyanine Green and 809-Nm Diode Laser. *Photomed. Laser Surg.* **2013**, *31* (4), 155–162. https://doi.org/10.1089/pho.2012.3430.

(13) Alves, E.; Faustino, M. A. F.; Neves, M. G.; Cunha, A.; Tome, J.; Almeida, A. An Insight on Bacterial Cellular Targets of Photodynamic Inactivation. *Future Med. Chem.* **2014**, *6* (2), 141–164. https://doi.org/10.4155/fmc.13.211.

(14) Kochevar, I. E.; Lambert, C. R.; Lynch, M. C.; Tedesco, A. C. Comparison of Photosensitized Plasma Membrane Damage Caused by Singlet Oxygen and Free Radicals. *Biochim. Biophys. Acta - Biomembr.* **1996**, *1280* (2), 223–230. https://doi.org/https://doi.org/10.1016/0005-2736(95)00297-9.

(15) Itri, R.; Junqueira, H. C.; Mertins, O.; Baptista, M. S. Membrane Changes under Oxidative Stress: The Impact of Oxidized Lipids. *Biophys. Rev.* **2014**, *6* (1), 47–61. https://doi.org/10.1007/s12551-013-0128-9.

(16) DeRosa, M. C.; Crutchley, R. J. Photosensitized Singlet Oxygen and Its Applications. *Coord. Chem. Rev.* **2002**, *233–234*, 351–371. https://doi.org/https://doi.org/10.1016/S0010-8545(02)00034-6.

(17) Estevão, B. M.; Pellosi, D. S.; De Freitas, C. F.; Vanzin, D.; Franciscato, D. S.; Caetano, W.; Hioka, N. Interaction of Eosin and Its Ester Derivatives with Aqueous Biomimetic Micelles: Evaluation of Photodynamic Potentialities. *J. Photochem. Photobiol. A Chem.* **2014**, *287*, 30–39. https://doi.org/10.1016/j.jphotochem.2014.04.015.

(18) Henderson, B. W.; Dougherty, T. J. How Does Photodynamic Therapy Work? *Photochem. Photobiol.* **1992**, *55* (1), 145–157. https://doi.org/10.1111/j.1751-1097.1992.tb04222.x.

(19) Gai, S.; Yang, G.; Yang, P.; He, F.; Lin, J.; Jin, D.; Xing, B. Recent Advances in Functional Nanomaterials for Light–triggered Cancer Therapy. *Nano Today* **2018**, *19*, 146–187. https://doi.org/https://doi.org/10.1016/j.nantod.2018.02.010.

(20) Aoki, P. H. B.; Schroder, A. P.; Constantino, C. J. L.; Marques, C. M. Bioadhesive Giant Vesicles for Monitoring Hydroperoxidation in Lipid Membranes. *Soft Matter* **2015**, *11* (30), 5995–5998. https://doi.org/10.1039/C5SM01019E.

(21) Aoki, P. H. B.; Morato, L. F. C.; Pavinatto, F. J.; Nobre, T. M.; Constantino, C. J. L.; Oliveira, O. N. Molecular-Level Modifications Induced by Photo-Oxidation of Lipid Monolayers Interacting with Erythrosin. *Langmuir* **2016**, *32* (15), 3766–3773. https://doi.org/10.1021/acs.langmuir.6b00693.

(22) Pereira, L. S. A.; Camacho, S. A.; Malfatti-Gasperini, A. A.; Jochelavicius, K.; Nobre, T. M.; Oliveira, O. N.; Aoki, P. H. B. Evidence of Photoinduced Lipid Hydroperoxidation in Langmuir Monolayers Containing Eosin Y. *Colloids Surfaces B Biointerfaces* **2018**, *171* (August), 682–689. https://doi.org/10.1016/j.colsurfb.2018.08.002.

(23) Mottola, M.; Caruso, B.; Perillo, M. A. Langmuir Films at the Oil/Water Interface Revisited. *Sci. Rep.* **2019**, *9* (1), 1–13. https://doi.org/10.1038/s41598-019-38674-9.

(24) Cruz Gomes da Silva, R. L.; Oliveira da Silva, H. F.; da Silva Gasparotto, L. H.; Caseli, L. How the Interaction of PVP-Stabilized Ag Nanoparticles with Models of Cellular Membranes at the Air-Water Interface Is Modulated by the Monolayer Composition. *J. Colloid Interface Sci.* **2018**, *512*, 792–800. https://doi.org/10.1016/j.jcis.2017.10.091.

(25) Salis, L. F. G.; Jaroque, G. N.; Escobar, J. F. B.; Giordani, C.; Martinez, A. M.;

Fernández, D. M. M.; Castelli, F.; Sarpietro, M. G.; Caseli, L. Interaction of 3′,4′,6′-Trimyristoyl-Uridine Derivative as Potential Anticancer Drug with Phospholipids of Tumorigenic and Non-Tumorigenic Cells. *Appl. Surf. Sci.* **2017**, *426*, 77–86. https://doi.org/10.1016/j.apsusc.2017.07.094.

(26) Schmidt, T. F.; Caseli, L.; Oliveira, O. N.; Itri, R. Binding of Methylene Blue onto Langmuir Monolayers Representing Cell Membranes May Explain Its Efficiency as Photosensitizer in Photodynamic Therapy. *Langmuir* **2015**, *31* (14), 4205–4212. https://doi.org/10.1021/acs.langmuir.5b00166.

(27) Bistaffa, M. J.; Kobal, M. B.; Souza, P. S. S.; Toledo, K. A.; Camacho, S. A.; Aoki, P. H. B. Photo-Induced Necrosis on Oropharyngeal Carcinoma (HEp-2) Cells Mediated by the Xanthene Erythrosine. *J. Nanosci. Nanotechnol.* **2020**, *20* (10), 6180–6190. https://doi.org/10.1166/jnn.2020.18123.

(28) Almeida, A. M.; Oliveira, O. N.; Aoki, P. H. B. Role of Toluidine Blue-O Binding Mechanism for Photooxidation in Bioinspired Bacterial Membranes. *Langmuir* **2019**, *35* (51), 16745–16751. https://doi.org/10.1021/acs.langmuir.9b03045.

(29) Bacellar, I. O. L.; Oliveira, M. C.; Dantas, L. S.; Costa, E. B.; Junqueira, H. C.; Martins, W. K.; Durantini, A. M.; Cosa, G.; Di Mascio, P.; Wainwright, M.; Miotto, R.; Cordeiro, R. M.; Miyamoto, S.; Baptista, M. S. Photosensitized Membrane Permeabilization Requires Contact-Dependent Reactions between Photosensitizer and Lipids. *J. Am. Chem. Soc.* **2018**, *140* (30), 9606–9615. https://doi.org/10.1021/jacs.8b05014.

(30) Bacellar, I. O. L.; Pavani, C.; Sales, E. M.; Itri, R.; Wainwright, M.; Baptista, M. S. Membrane Damage Efficiency of Phenothiazinium Photosensitizers. *Photochem. Photobiol.* **2014**, *90* (4), 801–813. https://doi.org/10.1111/php.12264.

(31) de Freitas, C. F.; Pellosi, D. S.; Estevão, B. M.; Calori, I. R.; Tsubone, T. M.; Politi, M. J.; Caetano, W.; Hioka, N. Nanostructured Polymeric Micelles Carrying Xanthene Dyes for Photodynamic Evaluation. *Photochem. Photobiol.* **2016**, *92* (6), 790–799. https://doi.org/10.1111/php.12645.

(32) Jori, G.; Fabris, C.; Soncin, M.; Ferro, S.; Coppellotti, O.; Dei, D.; Fantetti, L.; Chiti, G.; Roncucci, G. Photodynamic Therapy in the Treatment of Microbial Infections: Basic Principles and Perspective Applications. *Lasers Surg. Med.* **2006**, *38* (5), 468–481. https://doi.org/10.1002/lsm.20361.

(33) Sennato, S.; Bordi, F.; Cametti, C.; Coluzza, C.; Desideri, A.; Rufini, S. Evidence of Domain Formation in Cardiolipin-Glycerophospholipid Mixed Monolayers. A Thermodynamic and AFM Study. *J. Phys. Chem. B* **2005**, *109* (33), 15950–15957. https://doi.org/10.1021/jp051893q.

(34) Volpati, D.; Aoki, P. H. B.; Alessio, P.; Pavinatto, F. J.; Miranda, P. B.; Constantino, C. J. L.; Oliveira, O. N. Vibrational Spectroscopy for Probing Molecular-Level Interactions in Organic Films Mimicking Biointerfaces. *Adv. Colloid Interface Sci.* **2014**, *207* (1), 199–215. https://doi.org/10.1016/j.cis.2014.01.014.

(35) Camacho, S. A.; Kobal, M. B.; Almeida, A. M.; Toledo, K. A.; Oliveira, O. N.; Aoki, P. H. B. Molecular-Level Effects on Cell Membrane Models to Explain the Phototoxicity of Gold Shell-Isolated Nanoparticles to Cancer Cells. *Colloids Surfaces B Biointerfaces* **2020**, *194* (April), 111189. https://doi.org/10.1016/j.colsurfb.2020.111189.

(36) Rodrigues, R. T.; Morais, P. V.; Nordi, C. S. F.; Schöning, M. J.; Siqueira, J. R.; Caseli, L. Carbon Nanotubes and Algal Polysaccharides to Enhance the Enzymatic Properties of Urease in Lipid Langmuir-Blodgett Films. *Langmuir* **2018**, *34* (9), 3082–3093. https://doi.org/10.1021/acs.langmuir.7b04317.

(37) Sang, L.; Mudalige, A.; Sigdel, A. K.; Giordano, A. J.; Marder, S. R.; Berry, J. J.; Pemberton, J. E. PM-IRRAS Determination of Molecular Orientation of Phosphonic Acid Self-Assembled Monolayers on Indium Zinc Oxide. *Langmuir* **2015**, *31* (20), 5603–5613. https://doi.org/10.1021/acs.langmuir.5b00129.

(38) Scholl, F. A.; Morais, P. V.; Gabriel, R. C.; Schöning, M. J.; Siqueira, J. R.; Caseli, L. Carbon Nanotubes Arranged As Smart Interfaces in Lipid Langmuir-Blodgett Films Enhancing the Enzymatic Properties of Penicillinase for Biosensing Applications. *ACS Appl. Mater. Interfaces* **2017**, *9* (36), 31054–31066. https://doi.org/10.1021/acsami.7b08095.

(39) Yunoki, T.; Kimura, Y.; Fujimori, A. Maintenance Properties of Enzyme Molecule Stereostructure at High Temperature by Adsorption on Organo-Modified Magnetic Nanoparticle Layer Template. *Bull. Chem. Soc. Jpn.* **2019**, *92* (10), 1662–1671. https://doi.org/10.1246/bcsj.20190102.

(40) Marsh, D. Lateral Pressure in Membranes. *Biochim. Biophys. Acta - Rev. Biomembr.* **1996**, *1286* (3), 183–223. https://doi.org/10.1016/S0304-4157(96)00009-3.

(41) de Melo, W. de C. M. A.; Perussi, J. R. Comparando Inativação Fotodinâmica e Antimicrobianos. *Rev. Ciencias Farm. Basica e Apl.* **2012**, *33* (3), 331–340.

(42) Zhang, F.; Shi, F.; Ma, W.; Gao, F.; Jiao, Y.; Li, H.; Wang, J.; Shan, X.; Lu, X.; Meng, S. Controlling Adsorption Structure of Eosin y Dye on Nanocrystalline TiO 2 Films for Improved Photovoltaic Performances. *J. Phys. Chem. C* **2013**, *117* (28), 14659–14666. https://doi.org/10.1021/jp404439p.

(43) Alwin, S.; Sahaya Shajan, X.; Menon, R.; Nabhiraj, P. Y.; Warrier, K. G. K.; Mohan Rao, G. Surfacemodification of Titania Aerogel Films by Oxygen Plasma Treatment for Enhanced Dye Adsorption. *Thin Solid Films* **2015**, *595*, 164–170. https://doi.org/10.1016/j.tsf.2015.10.071.

(44) Takamoto, D. Y.; Lipp, M. M.; Von Nahmen, A.; Lee, K. Y. C.; Waring, A. J.; Zasadzinski, J. A. Interaction of Lung Surfactant Proteins with Anionic Phospholipids. *Biophys. J.* **2001**, *81* (1), 153–169. https://doi.org/10.1016/S0006-3495(01)75688-3.

(45) Hädicke, A.; Schwieger, C.; Blume, A. Cospreading of Anionic Phospholipids with Peptides of the Structure (KX)4K at the Air-Water Interface: Influence of Lipid Headgroup Structure and Hydrophobicity of the Peptide on Monolayer Behavior. *Langmuir* **2017**, *33* (43), 12204–12217. https://doi.org/10.1021/acs.langmuir.7b02255.

(46) Kaznessis, Y. N.; Kim, S.; Larson, R. G. Simulations of Zwitterionic and Anionic Phospholipid Monolayers. *Biophys. J.* **2002**, *82* (4), 1731–1742. https://doi.org/10.1016/S0006-3495(02)75525-2.

(47) Bialkowska, K.; Bobrowska-Hägerstrandb, M.; Hägerstrand, H. Expansion of Phosphatidylcholine and Phosphatidylserine/Phosphatidylcholine Monolayers by Differently Charged Amphiphiles. *Zeitschrift fur Naturforsch. - Sect. C J. Biosci.*

2001, *56* (9–10), 826–830. https://doi.org/10.1515/znc-2001-9-1024.

(48) Ruiz, G. C. M.; Pazin, W. M.; do Carmo Morato, L. F.; Oliveira, O. N.; Constantino, C. J. L. Correlating Mono- and Bilayers of Lipids to Investigate the Pronounced Effects of Steroid Hormone 17α-Ethynylestradiol on Membrane Models of DPPC/Cholesterol. *J. Mol. Liq.* **2020**, *311*, 113324. https://doi.org/10.1016/j.molliq.2020.113324.

(49) Gonçalves Da Silva, A. M.; Romão, R. I. S. Mixed Monolayers Involving DPPC, DODAB and Oleic Acid and Their Interaction with Nicotinic Acid at the Air-Water Interface. *Chem. Phys. Lipids* **2005**, *137* (1–2), 62–76. https://doi.org/10.1016/j.chemphyslip.2005.06.004.

(50) Iraolagoitia, X. L. R.; Martini, M. F. Ca2+ Adsorption to Lipid Membranes and the Effect of Cholesterol in Their Composition. *Colloids Surfaces B Biointerfaces* **2010**, *76* (1), 215–220. https://doi.org/10.1016/j.colsurfb.2009.10.037.

(51) Levin, I. W.; Thompson, T. E.; Barenholz, Y.; Huang, C. Two Types of Hydrocarbon Chain Interdigitation in Sphingomyelin Bilayers. *Biochemistry* **1985**, *24* (22), 6282–6286. https://doi.org/10.1021/bi00343a036.

(52) Rodrigues, J. C.; Caseli, L. Lipids Mediating the Interaction of Metronidazole with Cell Membrane Models at the Air-Water Interface. *Colloids Surfaces B Biointerfaces* **2018**, *171* (June), 377–382. https://doi.org/10.1016/j.colsurfb.2018.07.057.

(53) Gonçalves, G. E. G.; Morais, T. R.; Lago, J. H. G.; Caseli, L. Incorporation of Polygodial in Langmuir Films of Selected Lipids. *Thin Solid Films* **2019**, *669* (September 2018), 19–28. https://doi.org/10.1016/j.tsf.2018.10.025.

(54) Arrondo, J. L. R.; Goñi, F. M.; Macarulla, J. M. Infrared Spectroscopy of Phosphatidylcholines in Aqueous Suspension a Study of the Phosphate Group Vibrations. *Biochim. Biophys. Acta (BBA)/Lipids Lipid Metab.* **1984**, *794* (1), 165–168. https://doi.org/10.1016/0005-2760(84)90310-2.

(55) Geraldo, V. P. N.; Pavinatto, F. J.; Nobre, T. M.; Caseli, L.; Oliveira, O. N. Langmuir Films Containing Ibuprofen and Phospholipids. *Chem. Phys. Lett.* **2013**, *559*, 99–106. https://doi.org/10.1016/j.cplett.2012.12.064.

(56) Gericke, A.; Flach, C. R.; Mendelsohn, R. Structure and Orientation of Lung Surfactant SP-C and L-Alpha-Dipalmitoylphosphatidylcholine in Aqueous Monolayers. *Biophys. J.* **1997**, *73* (1), 492–499. https://doi.org/https://doi.org/10.1016/S0006-3495(97)78087-1.

(57) Liljeblad, J. F. D.; Bulone, V.; Tyrode, E.; Rutland, M. W.; Johnson, C. M. Phospholipid Monolayers Probed by Vibrational Sum Frequency Spectroscopy: Instability of Unsaturated Phospholipids. *Biophys. J.* **2010**, *98* (10), L50–L52. https://doi.org/10.1016/j.bpj.2010.02.009.

(58) Gomes, P. J.; Gonçalves Da Silva, A. M. P. S.; Ribeiro, P. A.; Oliveira, O. N.; Raposo, M. Radiation Damage on Langmuir Monolayers of the Anionic 1.2-Dipalmitoyl-Sn-Glycero-3-[Phospho-Rac-(1-Glycerol)] (Sodium Salt)(DPPG) Phospholipid at the Air-DNA Solution Interface. *Mater. Sci. Eng. C* **2016**, *58*, 576–579. https://doi.org/10.1016/j.msec.2015.09.017.

(59) González-Labrada, E.; Schmidt, R.; DeWolf, C. E. Kinetic Analysis of the Ozone Processing of an Unsaturated Organic Monolayer as a Model of an Aerosol

Surface. *Phys. Chem. Chem. Phys.* **2007**, *9* (43), 5814–5821. https://doi.org/10.1039/b707890k.

(60) Qiao, L.; Ge, A.; Osawa, M.; Ye, S. Structure and Stability Studies of Mixed Monolayers of Saturated and Unsaturated Phospholipids under Low-Level Ozone. *Phys. Chem. Chem. Phys.* **2013**, *15* (41), 17775–17785. https://doi.org/10.1039/c3cp52484a.

(61) Fringeli, U. P.; Müldner, H. G.; Günthard, H. H.; Gasche, W.; Leuzinger, W. The Structure of Lipids and Proteins Studied by Attenuated Total-Reflection (ATR) Infrared Spectroscopy. *Zeitschrift für Naturforsch. B* **2015**, *27* (7), 780–796. https://doi.org/10.1515/znb-1972-0712.